Earthquakes and Structures, *Vol. 21, No. 6 (2021) 653-667*
https://doi.org/10.12989/eas.2021.21.6.653

Experimental study on lateral behavior of precast wide beam-column joints

Jae Hyun Kim[1], Beom Soo Jang[2], Seung-Ho Choi[1], Yoon Jung Lee[3], Ho Seong Jeong[3] and Kang Su Kim*[3]

[1]*Department of Architectural Engineering, University of Seoul, 163 Siripdae-ro, Dongdaemun-gu, Seoul 02504, Korea*
[2]*Department of Structural Design, Dream Structural Engineering Co., 10 Dongtandae-ro 21-gil, Hwaseong-si, Gyeonggi-do 18471, Korea*
[3]*Department of Architectural Engineering and the Smart City Interdisciplinary Major Program, University of Seoul, 163 Siripdae-ro, Dongdaemun-gu, Seoul 02504, Korea*

(Received August 2, 2021, Revised October 21, 2021, Accepted November 10, 2021)

Abstract. In this study, cyclic loading tests were conducted on the precast concrete (PC) wide beam (WB)-column joints. Two beam-column joint specimens were fabricated with the arrangement and anchorage details of the reinforcing bars penetrating the beam and column as variables. Through a cyclic loading test, the lateral load-story drift ratio responses, seismic performance characteristics (e.g., ductility, overstrength factor), energy dissipation, strength and stiffness degradations of each specimen were compared and analyzed based on the various indices and the current structural codes (ACI 318-19 and ACI 374.1-05 report). In addition, the shear lag effect was confirmed through the gauge values of the PC beam, and the differences in seismic performance between the specimens were identified on that basis.

Keywords: beam-column joints; precast concrete; seismic performance; shear lag effect; wide beam

1. Introduction

With the recent growth of the global e-commerce market owing to spikes contact-free industries, the demand for logistics warehouses is rapidly increasing worldwide. Various construction methods have been applied to meet the increasing demand for logistics warehouses. Among them, the precast concrete (PC) construction method, which has the advantage of shortening the construction period, is emerging as an optimal alternative. However, in some countries, the cost of the framework for the PC system is often higher than that of a conventional reinforced concrete (RC) construction method, owing to the additional costs incurred from transportation and assembly in addition to the production costs of the PC member. Accordingly, in the PC industry, significant efforts are being made to improve the PC slabs, which account for a large proportion of the framework costs, so as to reduce the quantity of materials required for the production of PC members. However, the PC slabs developed so far are similar in concept and shape, and when applied to the same span length, the differences in the material quantities between the PC slabs are not significant (Rosenthal 1978, Arockiasamy *et al*. 1991, Mejia-McMaster and Park 1994, Tan *et al*. 1996, Natio *et al*. 2009). Therefore, in recent years, a wide beam (WB) system has attracted attention, as it can secure economic feasibility by reducing the required span length of a PC slab through the width of the WB member supporting the PC slab and lowering the individual floor height of the structure. However, in a general WB system, as certain longitudinal reinforcing bars of the beam penetrate the outside of the column section owing to the wide width of the beam, shear lag effects (Kulkarni and Li 2009, Gunasekaran and Ahmed 2014, Kuang *et al*. 2016) occur, resulting in degradation of the structural performance (i.e., flexural performance and lateral load resistance performance of the beam, etc.). For this reason, several standard design codes limit the application of WB systems by presenting criteria for the width of an WB manufactured using the RC method (RC-WB), as shown in Table 1 (Fadwa *et al*. 2014).

Although there are very few studies on WB manufactured using the PC method (PC-WB), many experimental and analytical studies have been conducted on RC-WB systems (Siah *et al.* 2003, Benavent-Climent 2007, Li and Kulkarni 2010, Mirzabagheri *et al.* 2016, Turker and Gungor 2018, Dabiri *et al.* 2019). Gentry *et al.* (1994) performed tests on RC-WB joints with the reinforcement details of the beam as variables, and Carlos *et al.* (2001) conducted an experimental study on an RC-WB system using the ratio of the beam to column width as the main variable. Fadwa *et al.* (2014) and Elsouri *et al.* (2015) performed cyclic loading tests on RC-WB joints and quantitatively evaluated their seismic performance, based on the comparative analysis with general RC beam-column joints. Behnam *et al.* (2018) developed a finite element model for simulating the behavior of RC-WB joints using ABAQUS, and performed a parametric study on the aspect ratios of the beams and columns and the number of reinforcing bars in the beam. A PC-WB system facilitates the quality control of members and implements the full PC method at the entire site with the PC slab, thereby reducing the construction time. However, a PC-WB system has a disadvantage in that it is difficult to secure the integrity of the beam-column joint relative to a general RC-WB system, as the beam and column members are individually

*Corresponding author, Professor
E-mail: kangkim@uos.ac.kr

ISSN: 2092-7614 (Print), 2092-7622 (Online)

Table 1 Wide beam width in code provisions

Code of practice	Year	Conditions
Eurocode 8	2004	$b_w \leq \min(b_c + h_b; 2b_c)$
NZS 3101	2006	$b_w \leq \min(b_c + h_c; 2b_c)$
ACI 318	2019	$b_w \leq \min(b_c + 1.5h_c; 3b_c)$

*Notations: b_w = beam width; b_c = column width; h_b = beam depth; h_c = column depth

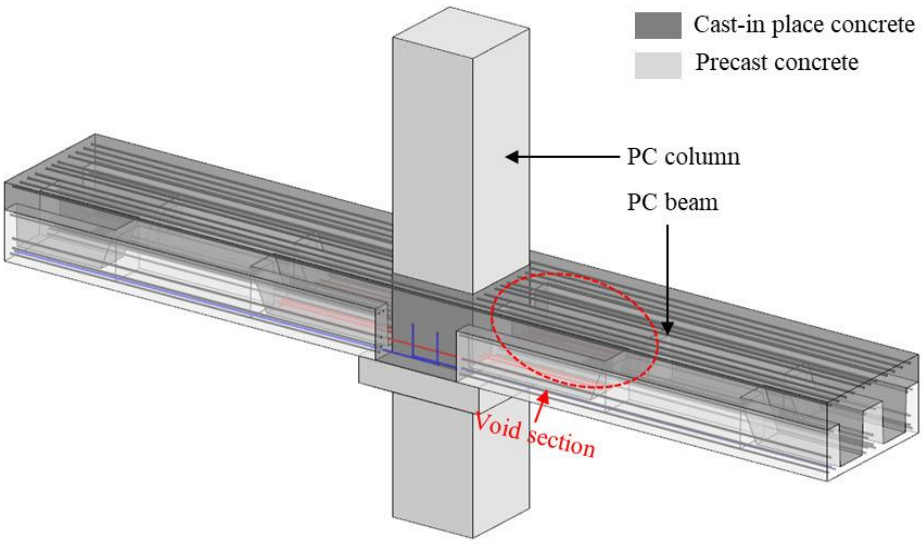

Fig. 1 Description of the wide beam-column joints

manufactured in the factory and assembled on site. Therefore, many studies are needed to ensure the integrity of the PC-WB system; however, very few studies have been conducted (Moon *et al.* 2007).

In this study, joint details comprising the PC column and PC-WB were developed as shown in Fig. 1. The proposed PC-WB system not only minimizes the quantity of materials required for the concrete owing to the presence of a void section in the longitudinal direction but also reduce the self-weight of the PC member, so as to facilitate lifting on the site. In addition, it can increase the structural integrity by pouring cast-in-place concrete into the void section at the PC-WB and beam-column joint, and ensures excellent buildability, as most of the reinforcing bars penetrating the beam and column can be placed in a straight line. (refer to Fig. 2) In this study, a quasi-static cyclic loading test was conducted on the developed PC-WB joint specimens, and the seismic performance evaluation of the PC-WB joints was conducted.

2. Experimental program

2.1 Test specimens

As shown in Figs. 2 and 3 and Table 2, two precast column-WB joint specimens were fabricated as a 1/2 scaled size of those used for typical logistics warehouses located in low-to-moderate seismic regions. Clear span length, and column height of the prototype were 8,420 mm and 4,020 mm, respectively. The details of the prototype wide beam were designed by considering dead load (2.7 kN/m^2) and lateral load (seismic zone factor = 0.11 g, site coefficient for short period = 1.12, site coefficient for long period = 0.84, and importance factor = 1.0) for the target logistics warehouse with 5 floors. Also, the prototype and specimens were designed to satisfy the details of the special moment frame presented in the ACI 318. Accordingly, the criteria for beam reinforcing details (clause 18.6 of ACI 318-19), column reinforcing details (clause 18.7 of ACI 318-19), and beam-column joint reinforcing details (clause 18.8 of ACI 318-19 except for 18.8.2.2) were checked. According to the clause 18.8.2.2 of ACI 318-19, the beam longitudinal reinforcement terminated in a joint shall extend to the far face of the joint core; however, the PC-WB joint presented in this study could not satisfy this clause because it had a unique shape (i.e., wide PC beam unit with a W-shape at the column-beam interface, and a M-shape at mid-span) different from typical RC beam-column joints. Variables of the specimens included the anchorage and reinforcing details of the bottom reinforcing bars penetrating the beam and column. As shown in Fig. 2(a), the total length (L_b) of the specimens was 6,100 mm, and the total height (H_c) was 3,125 mm. Figs. 2(b), 2(c), and 2(d) show that the beam width (b_w) was 950 mm, and the beam height before the placement of the topping concrete (h_{pc}) was 325 mm, whereas the beam height after the placement of the topping concrete (h) was 500 mm. The cross-section of the PC beam was made to have a W-shape (A-A' section in Fig. 2(b)) from the column-beam interface to the 900 mm section, and

Table 2 Summary of test specimens

Specimen		WB-H	WB-S
Beam †	Size	950 mm × 500 mm	
	Top reinforcing bars	11-D16	
	Bottom reinforcing bars	8-D13 (2-D13 hooked bars + 6-D13 straight bars)	8-D13 (8-D13 straight bars)
	Flexural strength, M_{nb} ††	394.8 kN·m (M_{nb1}=269.6 kN·m, M_{nb2}=519.9 kN·m)	
Column	Size	600 mm × 600 mm	
	Reinforcing bars	12-D19	
	Flexural strength, M_{nc}	750.9 kN·m	
Column overstrength factor, M_{nc} / M_{nb} (= λ_{ACI})		1.9	

† This shows the details of beam section at the interface of beam-column joints.

†† M_{nb}; The average of positive (M_{nb1}) and negative moment (M_{nb2})

a M-shape (B-B' section in Fig. 2(c)) for the remaining section, so as to reduce the material quantity and lifting weight. In the fabrication of the PC beam units, 8-Ø15.2 prestressing tendons were placed, and a prestress equivalent to approximately 0.6 times (0.6 f_{pu}) the ultimate strength of the tendons was introduced to control the beam deflection caused by the construction load. In addition, 6-D13 reinforcing bars were placed continuously over the entire length of the PC beam units in the lower parts. Also, 6-D16 reinforcing bars were placed on the top of the PC beam units to control the cracks at the time of prestressing tendons, creep and shrinkage, etc., and to hold stirrups during the fabrication and to reinforce the anchorage of stirrups.

In the upper part of the PC beam, 11-D16 straight bars were placed through the column over the entire span of the specimens when pouring the cast-in-place concrete. Meanwhile, D10 closed tie bars were used for stirrups in the PC beam; they were placed at 100 mm intervals in the A-A' section of the PC beam, and at 200 mm intervals in the remaining sections.

As shown in Fig. 2(d), the sectional size of the upper and lower PC columns was 600 × 600 mm; and the length of the upper column was 1,525 mm, excluding the beam-column joint in which the topping concrete was poured, whereas that of the lower column was 1,100 mm, including the corbel. In addition, 16-D22 longitudinal reinforcing bars were placed in the cross-sections of the upper and lower columns, respectively. At this time, splice sleeves were installed on the lower parts of all longitudinal reinforcing bars of the upper column, and the integrity of the upper and lower PC columns was secured by filling the splice sleeves with non-shrinkable mortar when assembling the upper and lower PC columns. D13 closed tie bars were used for stirrups in the PC column, and were placed at 50 mm intervals from the top of the upper PC column to the 450 mm section and bottom of the upper PC column to the 375 mm section, and at 100 mm intervals in the remaining sections. In addition, the stirrups of the lower PC column were placed at 50 mm intervals from the bottom to the 200mm section, and at 100 mm intervals in the remaining sections.

Figs. 2(e) and 2(f) show the details of the corbel as fabricated integrally with the lower PC column. The corbel was 950mm in width (b_{co}), 900 mm in depth (h_{co}), and 250 mm in height (H_{co}). In the cross-section of the corbel, D13 reinforcing bars were placed at 30 mm intervals in the vertical direction, and were assembled in the form of a grid with 100 mm spacing parallel to the column section of the specimen.

As shown in Fig. 3(a), the bottom of the PC beam of the WB-H specimen, 6-D13 straight bars were placed through the column, whereas 2-D13 hooked bars were placed with a development length of 400 mm outside the column section. As specified in ACI 318, the minimum development length (l_{hd}) of tensile deformed bars with standard hooks is 171.9 mm. For the 2-D13 hooked bars to be anchored to the outside of the joint, the panel zone area protruding outside the column section was filled with cast-in-place concrete. In addition, the distance from the center of the section to the center of the outermost reinforcing bar was 441 mm.

Fig. 3(b) shows that in the WB-S specimen, 8-D13 straight bars were placed through the column in the bottom of the PC beam without hooked bars, and the distance from the center of the section to the center of the outermost reinforcing bar was 311 mm. Unlike the WB-H specimen, the panel zone area protruding outside the column section of the WB-S specimen comprised PC extending from the beam (Area 1 in Fig. 3(b)), whereas the area between the column and protruding parts of the PC beam (Area 2 in Fig. 3(b)) was filled with cast-in-place concrete. As shown in Fig. 3(b), the PC beam units of the WB-S specimen protruded 295 mm from the beam-column interface and were fabricated in a U-shape, and both were placed at a separation distance of 10 mm from the center of the column. All other details were the same as those for the WB-H specimen.

Fig. 4 shows the fabrication process for the specimens. The PC beam and PC columns were individually manufactured. At the assembly stage, the PC beam units were then positioned in the corbel of the lower PC column, and the straight bars penetrating the beam-column joint were placed as shown in Fig. 4(c). Subsequently, the topping concrete was poured to integrate the lower PC column and PC beam units, as shown in Fig. 4(d) and the specimens were subjected to steam curing for a week. The upper and lower PC columns were then connected to complete the assembly, as shown in Fig. 4(e). The splice sleeves of the upper PC column were then filled with non-shrinkable mortar to ensure the integrity of the longitudinal

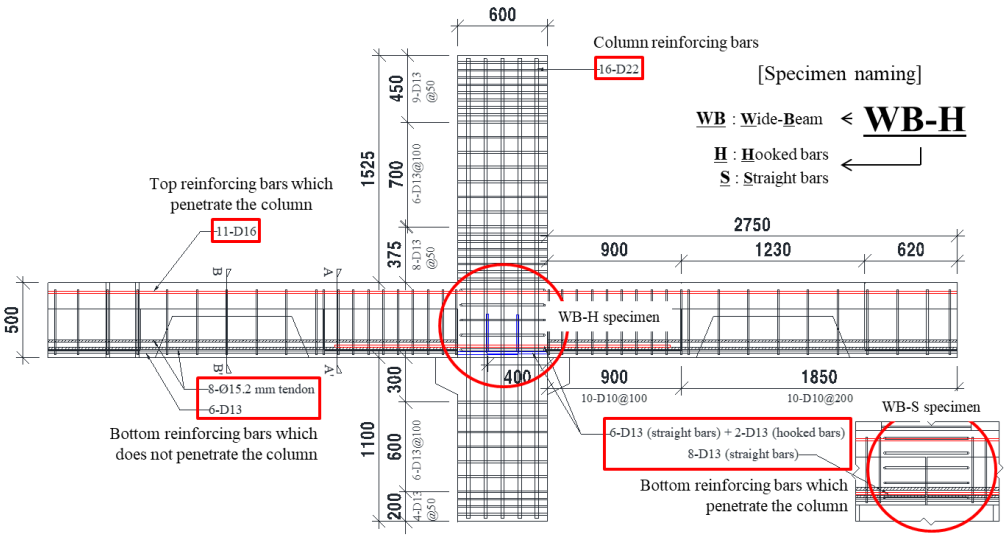

(a) Front view

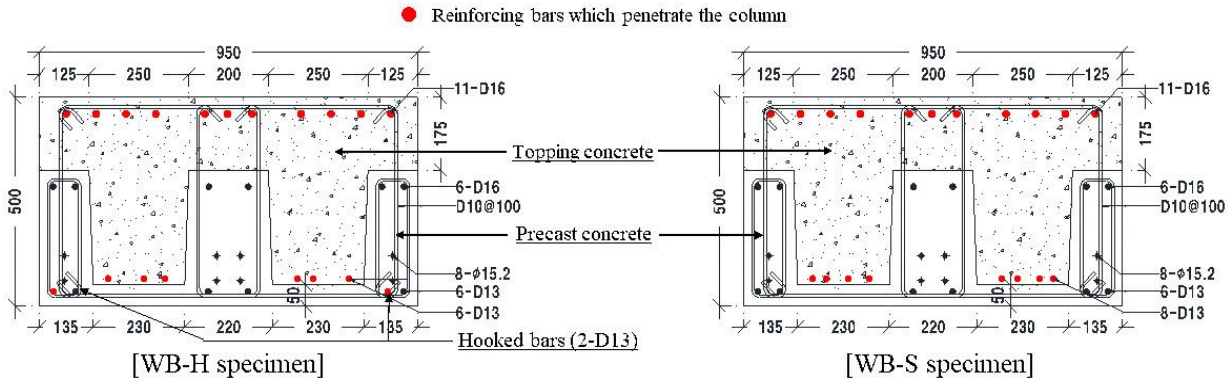

(b) beam section A-A'

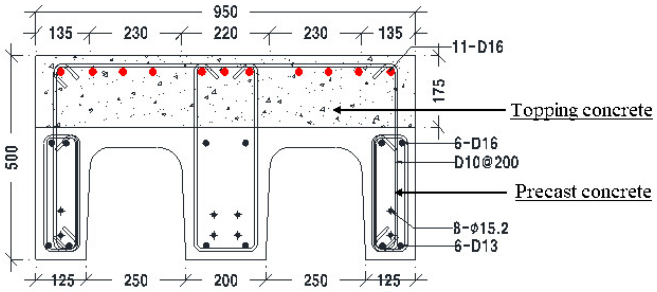

(c) beam section B-B'

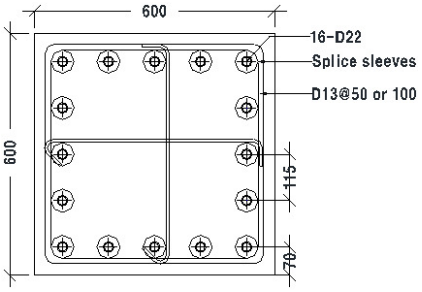

(d) column section

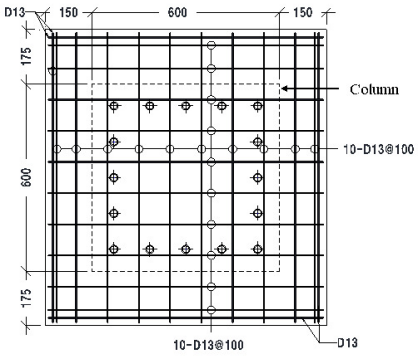

(e) corbel section

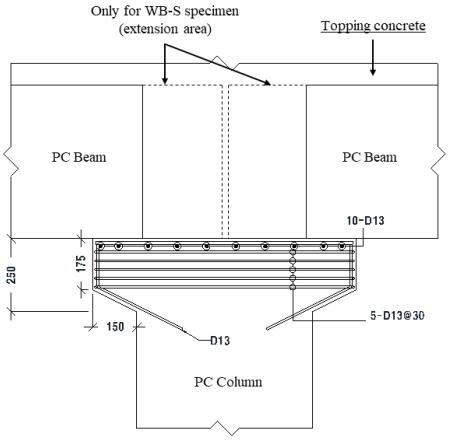

(f) corbel front view

Fig. 2 Dimensions and section details of test specimens (unit: mm)

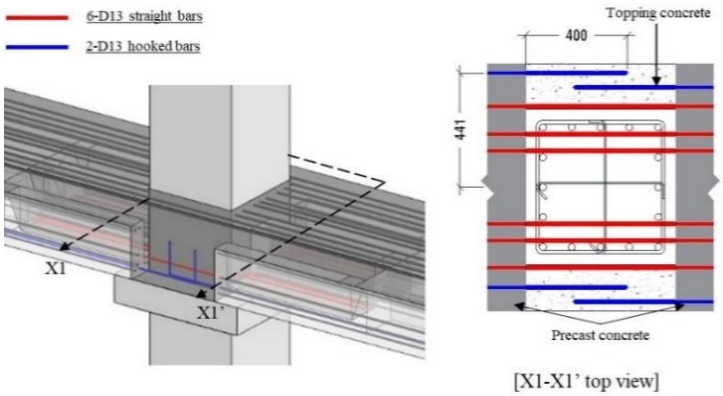

(a) WB-H specimen

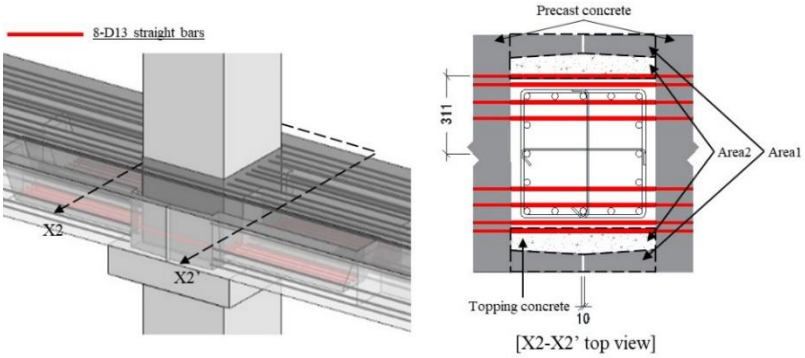

(b) WB-S specimen

Fig. 3 Longitudinal reinforced details at the interior joint (unit: mm)

Table 3 Material properties of test specimens (units in MPa)

Specimen	Compressive strength of concrete, f_{ck}		Yield strength of reinforcing bars (Tensile strength of reinforcing bars), $f_y(f_u)$				Yield strength of tendons (Tensile strength of tendons), $f_{py}(f_{pu})$
	PC	RC †	D10	D13	D16	D22	
WB-H WB-S	45.5	28.0	459.1(597.3)	456.5(618.0)	448.0(591.4)	454.2(599.8)	1,784.5(1,952.4)

† Cast-in-place concrete

reinforcing bars for the upper and lower PC columns.

2.2 Material properties

Table 3 lists the material test results for each specimen. The compressive test for the concrete and tensile tests of the reinforcing bars and tendons were conducted according to ASTM C39/C39M-21 and ASTM A370, respectively. It was found that the compressive strength of the concrete used for the PC member was 45.5 MPa, and that of the cast-in-place concrete was 23.4 MPa. The yield strength (f_y) of reinforcing bars ranged from 448.0 MPa to 459.1 MPa, and the tensile strength (f_u) ranged from 591.4 MPa to 618.0 MPa. The yield strength (f_{py}) and tensile strength (f_{pu}) of the prestressing tendons were 1,784.5 MPa and 1,952.4 MPa, respectively.

2.3 Test set-up and loading protocol

As shown in Fig. 5(a), both ends of the beam were fastened with two hinges to implement roller support, and the bottom of the column was set as a hinged support. In addition, a hydraulic jack was used to introduce a pre-axial load of 100 tonf, i.e., approximately 5.3% of the axial strength of the column (P_n = 1,871.5 tonf). The top of the column was connected to the actuator, and the lateral loading was applied using a displacement control method, according to the loading protocol shown in Fig. 5(b). This loading protocol complied with the provisions specified in the ACI 374.1 report 7.1, 7.2, 7.3 and 7.4. It is noted that the loading protocol is very important in seismic performance assessment of structures because it is supposed to reflect the time history of ground motions. (Rai 2001, Catalan *et al.* 2010). However, the goal of this study was to assess whether the seismic performance (i.e., integrated performance) of the joints in the proposed wide beam-column system satisfies the minimum requirements for the special moment resisting frame specified in the ACI 318-19, based on which a better way of its applications can be referenced.

As shown in Fig. 5(a), the distance (L_{eff}) between the roller supports of the beam was 5,100 mm, and the effective

(a) manufacturing PC beam units and PC columns

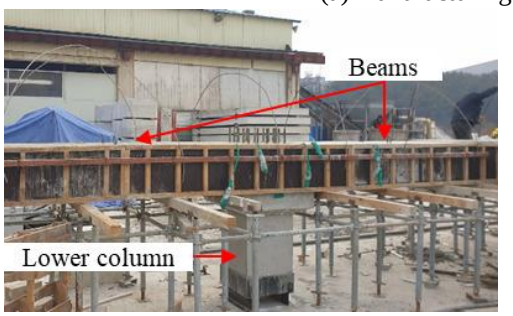

(b) assembling the beam and the lower column

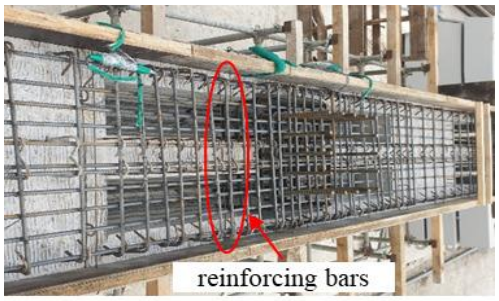

(c) placing reinforcing bars

(d) casting topping concrete

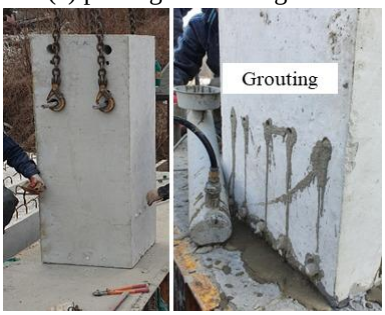

(e) assembling the beam and the upper column

Fig. 4 Fabrication process of test specimen

height (H_{eff}), which is the distance between the hinge support of the column and center of the loading point, was 3,070 mm.

As shown in Fig. 6(a), linear variable differential transformers (LVDTs) 1 and 2 were installed to measure the displacement of the loading point and that of the hinge frame located at the bottom of the column. The drift ratio (Δ) of the specimen was defined as follows:

$$\Delta = \frac{\left(\delta_{LVDT1} - \delta_{LVDT2}\right)}{H_{LVDT}} \approx \frac{\left(\delta_{act} - \delta_{slip}\right)}{H_{eff}} \quad (1)$$

where δ_{LVDT1} and δ_{LVDT2} are the horizontal displacements as measured using LVDT1 and LVDT2, respectively, and H_{LVDT} is the vertical distance between LVDT1 and LVDT2, which is 2,980 mm. In addition, δ_{act} represents the loading displacement of the actuator, and δ_{slip} represents the slip generated between the specimen and support frames. When the lateral load was applied to the specimen, the displacement of the actuator was controlled in real time, so that Δ could be the same as the target drift ratio shown in Fig. 5(b).

As shown in Fig. 6(b), strain gauges were attached at a distance of 200 mm from the beam-column interfaces to measure the longitudinal strain of the longitudinal top reinforcing bars penetrating the beam-column joint. However, the strain of the longitudinal bars could be different depending on the width direction of the beam, owing to the characteristics of the WB. Therefore, Gauge1 was attached 108 mm away from the column surface in the width direction, whereas Gauge2 was attached to the center of the column.

As summarized in Table 2, the nominal flexural strength of the PC beam (M_{nb}) and nominal flexural strength of the PC column (M_{nc}) as calculated from the material test results were 394.8 kN·m and 750.9 kN·m, respectively. In both specimens, the strength ratio of the column to the beam (M_{nc}/M_{nb}) was 1.9, and each specimen was designed such that the PC beam yielded before the PC column. Therefore, the nominal strength (Q_n) of the beam-column joint specimens could be defined as follows:

$$Q_n = \frac{\left(M_{nb1} + M_{nb2}\right)}{H_{eff}} \quad (2)$$

where M_{nb1} (= 269.5 kN·m) is the nominal flexural strength for the positive moment of the PC beam, and M_{nb2} (= 520.0 kN·m) is the nominal flexural strength for the negative

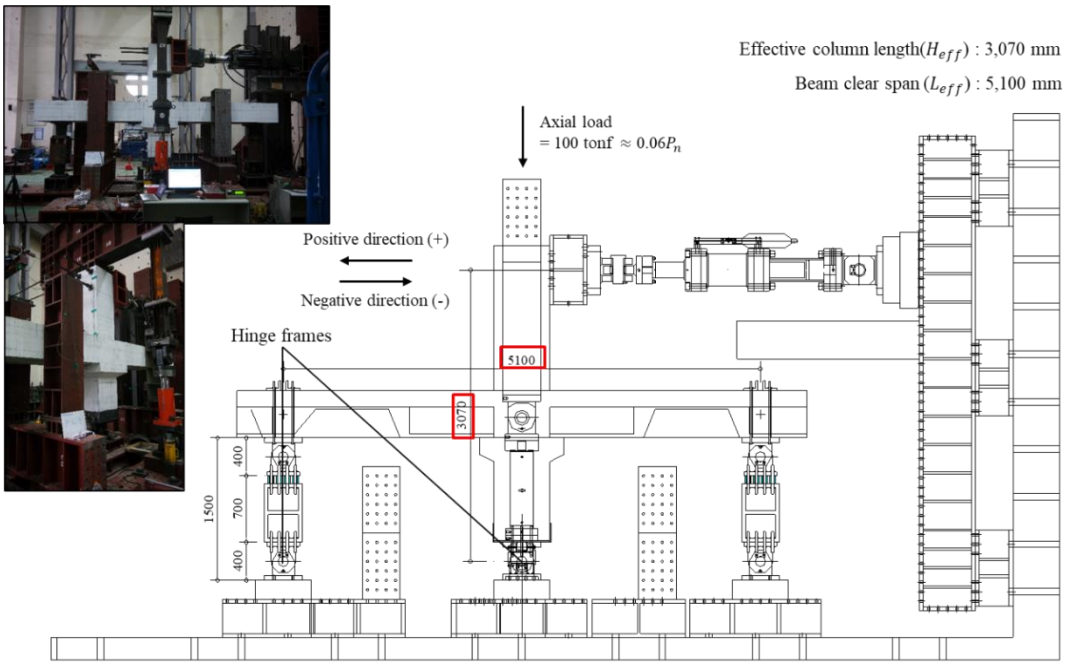

(a) test setup (unit: mm)

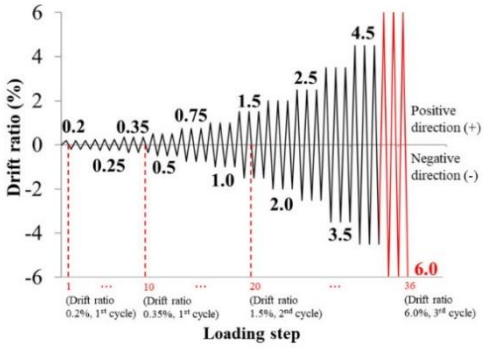

(b) Loading protocol

Fig. 5 Test setup and loading protocol

moment of the PC beam. The nominal strength, Q_n calculated using Eq. (2) was 257.4 kN for all specimens.

3. Experimental results

3.1 Lateral force responses

Fig. 7 shows the lateral responses according to the drift ratio of each specimen, and Fig. 8 shows the failure modes for each specimen. As shown in Fig. 7(a), in the WB-H specimen in which 2-D13 hooked bars extending from the beam were placed outside the column section, the initial vertical cracks occurred at the interface between the panel zone and PC beam ends at drift ratio of 0.2%. Simultaneously, the initial flexural cracks occurred at the ends of the PC beam. In addition, initial diagonal cracks in the panel zone were observed at drift ratio of 0.75%. The applied load reached the nominal strength (Q_n= ±257.4 kN) at drift ratio of 0.67% and -1.86%. It is noted that the difference in the maximum applied load of each load step for the drift ratio from -0.75% to -2.0% was at the level of 6%, indicating that there is no significant difference in the point of the drift ratio for Q_n in the positive and negative directions. The maximum loads (Q_{max}) of the specimen were found to be 296.4 kN and -262.0 kN at drift ratios of 1.46% and -1.99%, respectively. These values correspond to 1.15 and 1.02 times the nominal strength (Q_n) of the WB-H specimen calculated using Eq. (2). Concrete crushing was observed in some areas at the end of the PC beam at drift ratio of 3.5%, and the applied load began to decrease at drift ratio of 4.5%. At drift ratio of 6.0%, a large portion of concrete at the end of the PC beam underwent crushing (refer to Fig. 8(a)) and showed the significant level of strength degradation in the successive cycles. In the 3rd cycle with drift ratio of 6.0%, the maximum applied load of the specimen was 53% and 57% of the maximum strength in the positive and negative directions, respectively. Fig. 7(b) shows that in the WB-S specimen with straight bars penetrating the beam and column, cracks occurred along the interface between the PC beam units located in the panel zone at drift ratio of 0.2%, and interfacial cracks in both PC beams and subsequent diagonal cracks occurred at drift ratio of 0.25%. In addition, initial flexural cracks

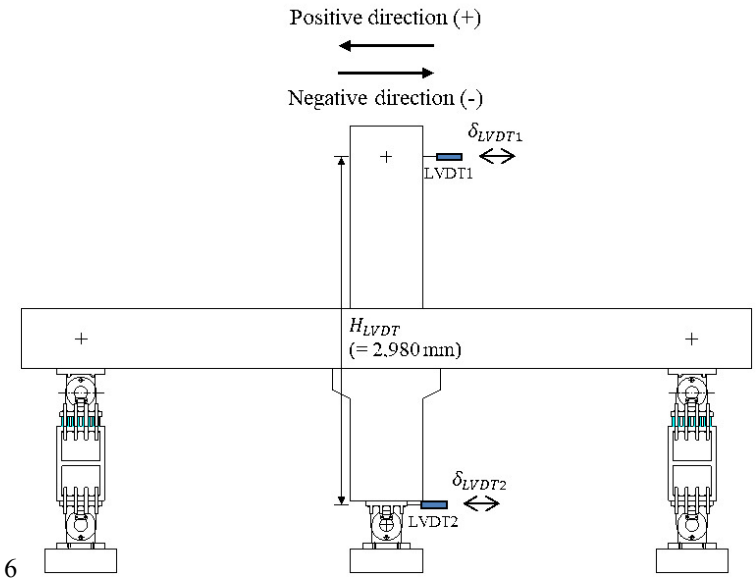

(a) LVDTs

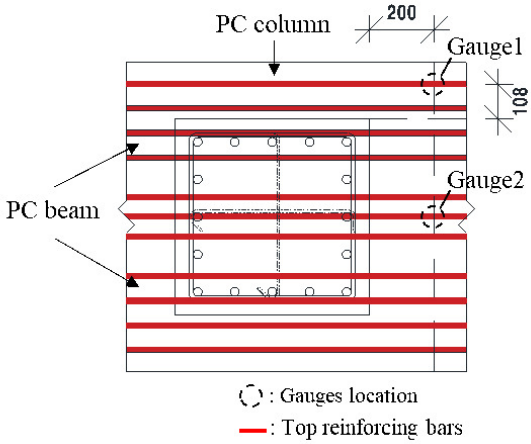

(b) Gauges

Fig. 6 Measurement of displacement and strains

occurred at the ends of both PC beams at drift ratio of 0.35%. The applied load of the specimen reached the nominal strength (Q_n = ±257.4 kN) at drift ratios of 0.72% and -0.85%. The maximum loads (Q_{max}) of the WB-S specimen were found to be 320.6 kN and -293.5 kN at drift ratios of 1.48% and -1.49%, respectively. These values correspond to 1.25 and 1.14 times the nominal strength (Q_n) of the WB-S specimen in the positive and negative directions, respectively. At drift ratio of 2.5%, the concrete in the panel zone peeled off. Similar to the WB-H specimen, a large portion of concrete at the end of the PC beam was crushed showing a significant level of strength degradation in the successive cycles at drift ratio of 6.0% (refer to Fig. 8(b)). In the 3rd cycle with drift ratio of 6.0%, the maximum applied load of the specimen was found to be 64% and 51% of the maximum strength in the positive and negative directions, respectively. In the WB-S specimen, as shown in Fig. 8(b), significant concrete spalling was observed at the end of the PC beam parallel to the panel zone. However, no damage was found in the internal panel zone surrounded by the PC beam units (refer to Fig. 8(c)).

3.2 Ductility

Fig. 9(a) shows the skeleton curve of the specimens for each cycle (e.g., 1st cycle, 2nd cycle, and 3rd cycle). The yield point (Δ_y) of the specimens was determined based on the ACI 374.2 report 4.7 (2013) for the 1st cycle of all loading steps as shown in Fig. 9(b), where Q_y is the yield strength of the test specimens, K_e is the effective elastic stiffness, Δ_e is the drift ratio under the load of αQ_y, and α is the fraction of Q_y used to define the idealized effective elastic stiffness; a value of 0.75 is generally used for flexure-dominant elements. In this study, the ultimate point (Δ_u) of the specimens was defined as the point reduced to less than 80% of the maximum strength for the 3rd cycle of all loading steps. Table 4 shows the yield point (Δ_y), ultimate point (Δ_u), and ductility ($\mu = \Delta_u / \Delta_y$) of each specimen in the positive and negative directions, respectively. The WB-H specimen reached the yield point at drift ratio of 0.58% in the positive direction and of 0.56% in the negative direction, and reached the ultimate point at drift ratio of 4.24% in the positive direction and of 4.02% in

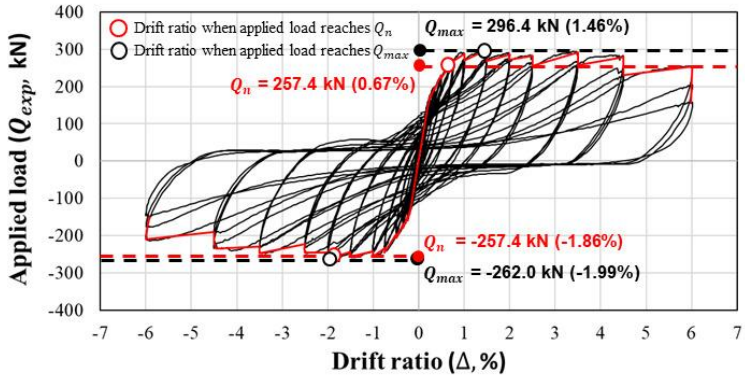

(a) WB-H specimen

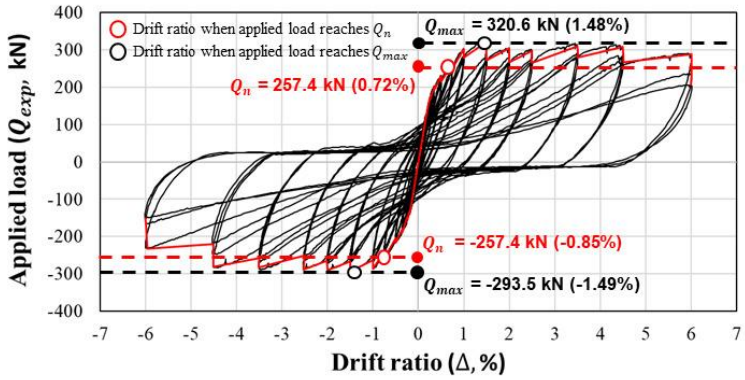

(b) WB-S specimen

Fig. 7 Applied load-drift ratio curves of test specimens

the negative direction. The ductility of the WB-H specimen was 7.31 in the positive direction and 7.18 in the negative direction. The WB-S specimen reached the yield point at drift ratio of 0.64% and 0.65% in the positive and negative directions, respectively, and reached the ultimate point at drift ratio of 4.75% and 4.11% in the positive and negative directions, respectively. The ductility of the WB-S specimen was 7.42 in the positive direction and 6.32 in the negative direction. The ductility of all specimens was smaller than the response modification factor (R = 8) of the RC special moment frame and larger than that (R = 5.5) of the intermediate RC moment frame as specified in ASCE (2010). In other words, the developed WB system exhibited a ductile behavior higher than the ductility level for an intermediate RC moment frame stipulated in the current structural codes.

3.3 Overstrength factor

Table 5 shows the maximum applied load (Q_{max}), nominal strength (Q_n), and corresponding overstrength factors ($\Omega_n = Q_{max} / Q_n$) for each specimen in the positive and negative directions. The corresponding overstrength factors (Ω_n) of the WB-H specimen were 1.15 in the positive direction and 1.02 in the negative direction, whereas those Ω_n of the WB-S specimen were 1.25 in the positive direction (109% of the WB-H specimen) and 1.14 in the negative direction (112% of the WB-H specimen). ACI 318 presents the acceptance criteria for the column overstrength factor ($\lambda_{ACI} = \sum M_{nc} / \sum M_{nb}$ refer to Table 2) greater than 1.2 in an RC special moment frame. In ACI 374.1 report 9.1.2, it was suggested that for special-shaped beam-column joints (e.g., precast joints) that cannot meet the minimum requirements of the RC special moment frame as specified in ACI 318, so as to be considered to have the same level of structural performance as the RC special moment frame, the acceptance criteria should be as follows.

$$\Omega_n \leq \lambda_{ACI} \tag{3}$$

This is a criterion to limit the Ω_n value while considering the overstrength of the materials to be smaller than the λ_{ACI} value, and to thereby minimize damage to the column owing to an unexpected increase in the strength of the beam. It was found that for the aforementioned acceptance criteria, the WB-H specimen secured a safety margin of 0.75 (= 1.9 − 1.15; $\lambda_{ACI} - \Omega_n$) in the positive direction and 0.88 in the negative direction, and the WB-S specimen 0.65 in the positive direction and 0.76 in the negative direction, as summarized in Table 2 and 5. Consequently, all specimens met the acceptance criteria, or Eq. (3), as presented in the ACI 374.1 report 9.1.2.

3.4 Energy dissipation

The energy dissipation performance of the structural members is the main parameter for evaluating the seismic

(a) WB-H specimen

(b) WB-S specimen

(c) Panel zone in WB-S specimen

Fig. 8 Failure mode of test specimens

Table 4 Ductility of test specimens

Specimens	Load directions	Δ_y [%]	Δ_u [%]	$\mu_e = \Delta_u / \Delta_y$
WB-H	positive direction (+)	0.58	4.24	7.31
	negative direction (-)	-0.56	-4.02	7.18
WB-S	positive direction (+)	0.64	4.75	7.42
	negative direction (-)	-0.65	-4.11	6.32

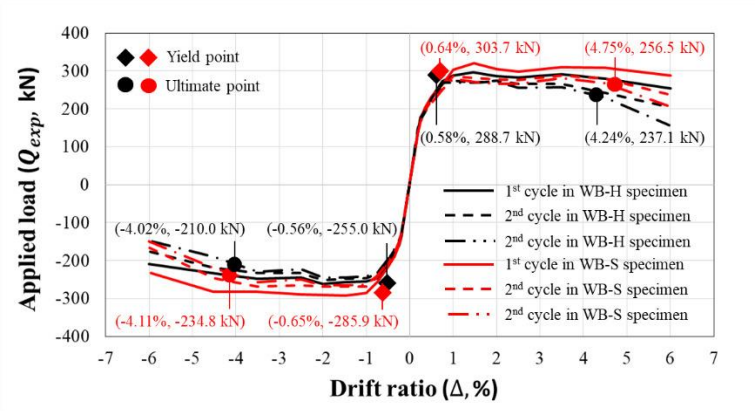

(a) skeleton curve

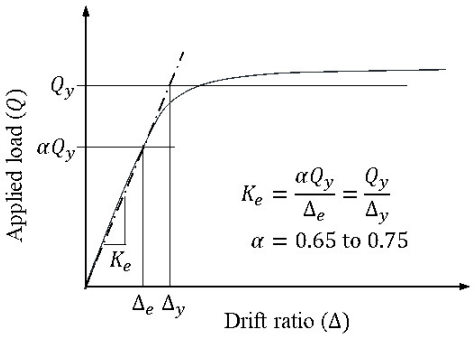

(b) determination of yield point

Fig. 9 Skeleton curve and yield point of test specimens

response of an entire structure (Choi *et al.* 2018, Yang *et al.* 2018, Karayannis and Golias 2003, Zhang *et al.* 2020, Kim *et al.* 2021). In this study, the energy dissipation performance of each specimen was analyzed using the energy dissipation ratio (β_{ACI}) presented in the ACI 374.1 report 9.1.3-2 as shown in Fig. 10(a).

$$\beta_{ACI,i} = \frac{E_{h,i}}{\left(Q_{\max 1,i} + Q_{\max 2,i}\right)\left(\Delta_{1.i}^{'} + \Delta_{2.i}^{'}\right)} \quad (4)$$

In the preceding equation, $E_{h,i}$ is the dissipated energy determined using the internal area of the hysteresis curve of each loading step, and $Q_{max\ 1,i}$ and $Q_{max\ 2,i}$ are the maximum applied loads in the positive and negative directions, respectively, at the same cycle. $\Delta'_{1,i}$ and $\Delta'_{2,i}$ can be calculated as follows:

$$\Delta_i^{'} = \Delta_i - \frac{Q_{\max,i}}{K_I} \quad (5)$$

Table 5 Overstrength factor of test specimens

Specimens	Load directions	Q_n [kN] (Corresponding drift ratio, %)	Q_{max} [kN] (Corresponding drift ratio, %)	$\Omega_n = Q_{max} / Q_n$
WB-H	positive direction (+)	257.4 (0.67%)	296.4 (1.46%)	1.15
	negative direction (-)	-257.4 (-1.86%)	-262.0 (-1.99%)	1.02
WB-S	positive direction (+)	257.4 (0.72%)	320.6 (1.48%)	1.25
	negative direction (-)	-257.4 (-0.86%)	-293.5 (-1.49%)	1.14

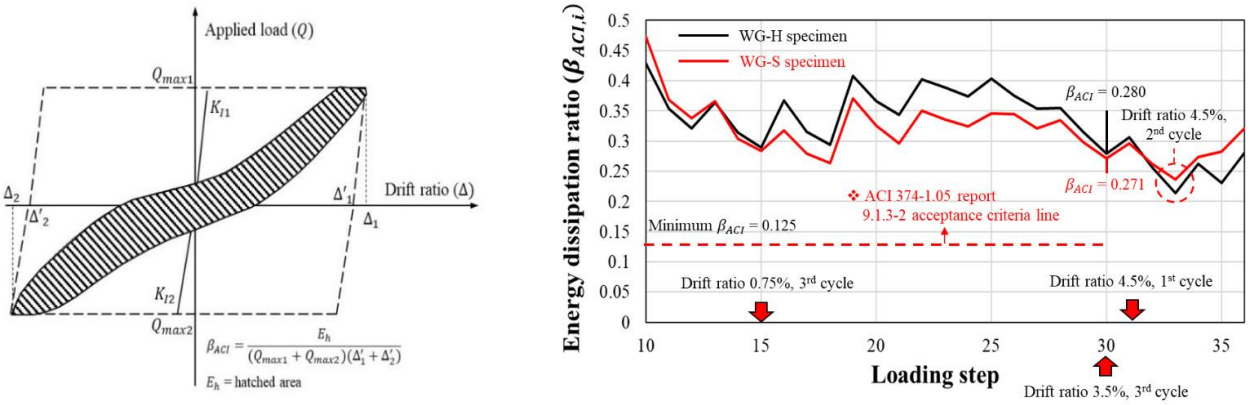

(a) determination of energy dissipation ratio (b) energy dissipation ratio

Fig. 10 Energy dissipation ratio of test specimens

where Δ_i is the drift ratio at $Q_{max,i}$, and K_I is the initial stiffness of the specimen as defined at drift ratio of 0.35%. Fig. 10(b) shows the energy dissipation ratio ($\beta_{ACI,i}$) of each specimen at the loading step after drift ratio of 0.35% (3rd cycle, loading step: 9). The changes in the energy dissipation ratio of each specimen similar up to drift ratio of 0.75% (3rd cycle, loading step: 15). In the drift ratios ranging from 1.0% (1st cycle, loading step: 16) to 4.5% (1st cycle, loading step: 31), the WB-H specimen showed a relatively higher energy dissipation performance. However, the energy dissipation ratio of the WB-H specimen decreased rapidly at drift ratio of 4.5% (1st cycle, loading step: 31). Consequently, the WB-S specimen showed a relatively higher energy dissipation performance relative to the WB-H specimen after drift ratio of 4.5% (2nd cycle, loading step: 32). This will be discussed further below.

In Fig. 10(b), the red dotted line indicates the acceptance criteria from the ACI 374.1 report 9.1.3-2. This means that for special-shaped beam-column joints such as PC beam-column joints to have an energy dissipation performance equivalent to that of the RC special moment frame, $\beta_{ACI,i}$ should be greater than 0.125 until the 3rd cycle of drift ratio of 3.5%. As a result, the values of β_{ACI} of each specimen at drift ratio of 3.5% (3rd cycle, loading step: 30) were 0.280 and 0.271 for the WB-H and WB-S specimens, respectively, which is more than twice the acceptance criteria (0.125). That is, the WB system proposed in this study has an energy dissipation performance higher than that of the RC special moment frame.

3.5 Strength degradation

In general, beam-column joints can be regarded as primary elements with significant impacts on the seismic behavior of the entire frame. Therefore, the beam-column joint should ensure a high level of residual strength, even after the frame is subjected to the ultimate load (Chiu *et al.* 2019, Nguyen *et al.* 2020, Al-Osta *et al.* 2020). In this study, the strength degradation of each specimen was quantitatively compared using the strength degradation index (*StrI*) as presented in the ACI 374.1 report 9.1.3-1. The strength degradation index (*StrI*) can be calculated as follows.

$$StrI_i = \frac{Q_{\max,i}}{Q_{\max}} \tag{6}$$

where $Q_{max,i}$ is the maximum applied load for each loading step. Fig. 11 shows the strength degradation index for the loading steps after the maximum applied load (Q_{max}). As the drift ratio increased, the $StrI_i$ values of the two specimens tended to be similar.

The ACI 374.1 report 9.1.3-1 stipulates that the strength degradation of a specimen should not exceed 25% before the 3rd cycle of drift ratio of 3.5%. The red dotted line in Fig. 11 indicates the acceptance criteria according to the ACI 374.1 report 9.1.3-1, which is a $StrI_i$ value of 0.75. The $StrI_i$ values of both specimens were 0.87 in the positive direction and 0.88 in the negative direction at drift ratio of 3.5% (3rd cycle, loading step: 30), respectively. These results suggest that the two specimens met the corresponding criteria. Therefore, it can be said that the WB system proposed in this study has a strength degradation performance equal to or that of the RC special moment frame.

3.6 Stiffness performance

In this study, the stiffness performance of the WB system was evaluated based on the ACI 374.1 report 9.1.1 and ACI

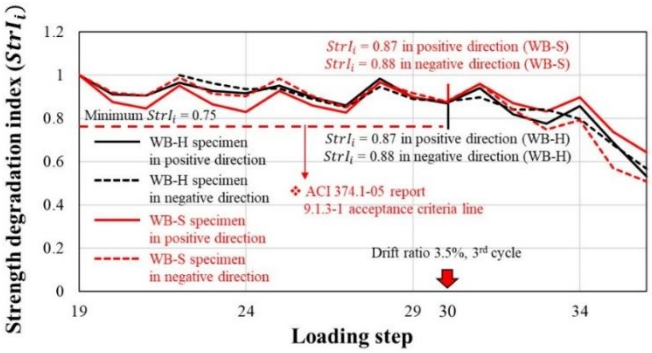

Fig. 11 Strength degradation index of test specimens

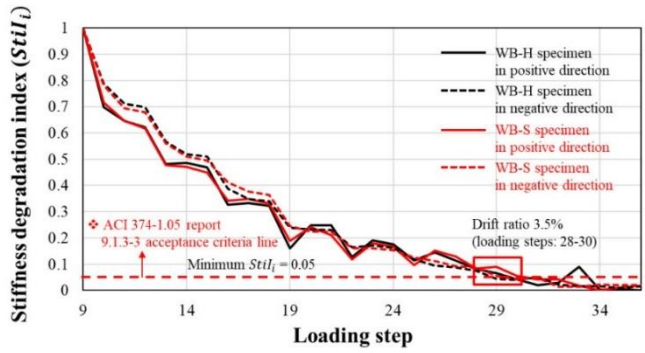

(a) StiI from loading steps 9 to 36

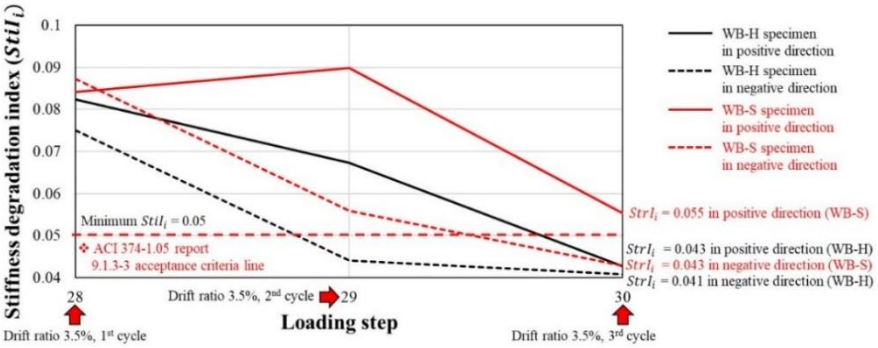

(b) Enlarged view of StiI from loading steps 28 to 30

Fig. 12 Stiffness degradation index of test specimens

374.1 report 9.1.3-3. The ACI 374.1 report 9.1.1 prescribes that a specimen should develop the design strength (ϕQ_n; ϕ=1.0) before reaching the allowable drift ratio (Δ_{allow}). This can be represented in terms of the stiffness, as follows.

$$k_{\exp,\phi Q_n} > k_n = \frac{\phi Q_n}{\Delta_{allow}} \tag{7}$$

where $k_{\exp,\phi Qn}$ is the secant stiffness when the specimen reached Q_n. k_n is the demand stiffness of the specimen as determined by ϕQ_n and Δ_{allow}, and the value of k_n is 4.19 kN/mm for all specimens. Considering that the application of the WB system developed in this study is applied in logistic warehouses, Δ_{allow} was set to 2.0 %, corresponding to the structure for seismic category Ⅱ as presented in IBC (2018).

The $k_{\exp,\phi Qn}$ of the WB-H specimen was 299% of k_n (i.e., $k_{\exp,\phi Qn}$=12.51 kN/mm) in the positive direction and 108 % (i.e., $k_{\exp,\phi Qn}$=4.51 kN/mm) in the negative direction. Meanwhile, the $k_{\exp,\phi Qn}$ of the WB-S specimen was 278% of k_n in the positive direction and 233% in the negative direction, respectively. That is, both specimens met the initial stiffness criteria for RC special moment frame specified as specified in ACI 374.1 report 9.1.1. However, in the WB-H specimen, the $k_{\exp,\phi Qn}$ value was relatively small in the negative direction as the maximum load was exerted at a relatively high drift ratio, as mentioned earlier.

In this study, the stiffness index (*StiI*) was introduced to compare and analyze the stiffness degradation characteristics according to the loading steps as follows.

$$StiI_i = \frac{k_{si}}{K_I} \tag{8}$$

where k_{si} is the secant stiffness from story drift ratio of 0.35% to -0.35% at each loading step. Fig. 12(a) shows the

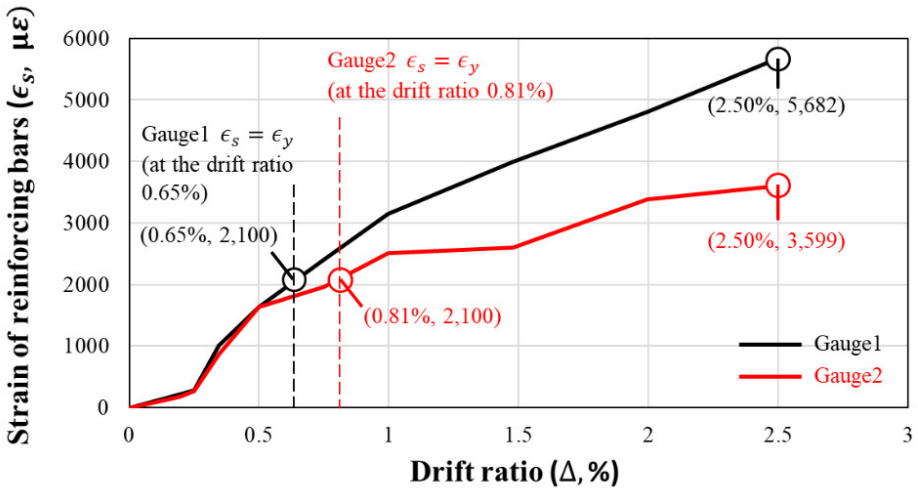

Fig. 13 Strain of top reinforcing bars in beams obtained from gauges

values of $StiI_i$ for each specimen according to the loading steps, and Fig. 12(b) shows an enlarged view of the $StiI_i$ values at drift ratio of 3.5% (i.e., loading steps from 28 to 30). In the ACI 374.1 report 9.1.3-3, it is specified that the $StiI_i$ of a specimen should be greater than 0.05 at the 3rd cycle of drift ratio of 3.5%, and this criterion was indicated with red dotted lines as shown in Fig. 12. The $StiI_i$ of the WB-S specimen was 0.055 in the positive direction and 0.043 in the negative direction at drift ratio of 3.5%. Accordingly, the aforementioned criteria were met only in the positive direction. In contrast, the $StiI_i$ of the WB-H specimen was 0.043 in the positive direction (78% of the WB-S specimen) and 0.041 in the negative direction (95% of the WB-S specimen), thus the $StiI_i$ criteria were not met. This is addressed further in the discussion below.

4. Discussions

4.1 Shear lag effect

When the width of the beam is larger than that of the column to a certain degree as in the WB system, the reinforcing bars located in the entire cross section of the beam may not experience the same strain in the width direction of the beam, owing to the shear lag effect (Kulkarni and Li 2009, Gunasekaran and Ahmed 2014). Particularly in the case of PC members for which the integrity of joints (i.e., the development performance of the main bars) is important for transmitting member forces between the PC members, the reinforcing bars experiencing load resistance at a relatively early time bear more of the required bond stress than the other reinforcing bars. Consequently, the demand bond stress is concentrated on the reinforcing bars activated first, and this may cause the early bond loss of these reinforcing bars, leading to the deterioration of integrity between the structural members (Kuang *et al.* 2016).

Fig. 13 shows the strain data (ε_s) as measured from the gauges 1 (i.e., the gauge attached to the outermost reinforcing bar) and 2 (i.e., the gauge attached to the center reinforcing bar in the cross-section) shown in Fig. 6(b) at drift ratio of 0.2%, 0.25%, 0.35%, 0.5%, 0.75%, 1.0%, 1.5%, 2.0% and 2.5%, respectively. Unfortunately, as the gauges of the WB-H specimen were lost owing to premature damage, only the data of the WB-S specimen are shown in Fig. 13. Both the outermost reinforcing bar and center reinforcing bar in the cross-section show relatively similar values up to drift ratio of 0.5%, after which the center reinforcing bar in the section underwent a higher strain than the outermost reinforcing bar. In particular, the outermost reinforcing bar underwent a strain of 0.0018 at drift ratio of 0.65%, the point at which the center reinforcing bar in the section reached the yield strain (ε_y=0.0021). The outermost reinforcing bar reached the yield strain at drift ratio of 0.81%. It is noted that the yield point (Δ_y) of the WB-S specimen according to the ACI 374.2 report 4.7 described in Fig. 9(b) is 0.64% as shown in Table 4, which is very similar to the 0.65% drift ratio at the point when the center reinforcing bar in the cross-section reached the yield strain (ε_y=0.0021). At drift ratio of 0.5%, the center strain in the section underwent a strain of 0.0057, whereas the outermost reinforcing bar underwent a strain of 0.0036. That is, it is estimated that a relatively larger deformation occurs in the center of the beam section relative to that in the outer end of the WB, owing to the shear lag effect before and after the yield point of the beam. That is, in the WB system, it is estimated that the center of the beam section experiences a relatively larger deformation than the outer end before and after the yielding of the beam, owing to the shear lag effect.

4.2 Design implication

In this study, the top reinforcing bars (i.e., 11-D16) of the specimens were integrally placed across the entire span to penetrate the column section, whereas only some of the bottom reinforcing bars penetrated the column section or past the sides of the column in placing the topping concrete. That is, as shown in Figs. 2 and 3, for the WB-H specimen, the 6-D13 bottom reinforcing bars penetrated the column and the 2-D13 bottom reinforcing bars passed through the

side of the column. In contrast, in the case of the WB-S specimen, all of the bottom reinforcing bars (8-D13 bars) were reinforced through the column. In general, if the anchorage details of the reinforcing bars continuously placed in the PC column and PC beam members of the PC system are undesirable, or if damage occurs to the concrete surrounding the reinforcing bars owing to a large strain, slip may occur owing to the bond loss of the reinforcing bars, leading to the stiffness degradation of the beam-column joints. The test specimens used in this study were found to meet the initial stiffness criterion specified in ACI 374.1 report 9.1.1. However, although the stiffness degradation criterion presented in the ACI 374.1 report 9.1.3-3 was met in the positive direction of the WB-S specimen, the criterion was not met in both the positive and negative directions of the WB-H specimen. That is, it is assumed that the specimens meet the initial stiffness criterion; however, slip occurs owing to the damage to the concrete surrounding the reinforcing bars in the high displacement stage (e.g., drift ratio of 3.5%, 3rd cycle). The slip of the reinforcing bars is also closely related to the energy dissipation performance of the joint. In other words, when slip occurs, the plastic behavior of the reinforcing bars is limited, and the energy dissipation performance also decreases. As mentioned earlier, the WB-H specimen showed a rapid decrease in the energy dissipation performance after drift ratio of 3.5% (1st cycle, loading step: 29). It is estimated that the shear lag effect is relatively higher in the WB-H specimen than in the WB-S specimen. This is because the distance in the direction of width between the outermost bottom reinforcing bars penetrating the beam and column of the WB-H specimen was 882.0 mm, whereas that in the WB-S specimen was 622.0 mm as shown in Fig. 3. For the PC-WB system proposed in this study to meet all of the ACI 374.1 report, the bottom reinforcing bars penetrating the beam and column should be placed within the appropriate effective flange width (b_{eff}). However, the number of test specimens in this study was small, and the measurement information of the gauges attached across the width of the specimen was insufficient, further experimental research is needed to identify the b_{eff} of the PC-WB.

5. Conclusions

In this study, PC WB-column joint specimens were fabricated with the arrangement and anchorage details of reinforcing bars penetrating the beam and column as variables, and the quasi-static cyclic loading tests were performed. Based on the various indices and response data obtained from the ACI 374.1 report and gauges, the seismic performance of the developed PC-WB specimens was compared and analyzed in detail. Based on this, the following conclusions can be drawn:

• The maximum load (Q_{max}) of all specimens showed values that exceeding the nominal strength (Q_n) as calculated based on ACI 318. The specimens failed owing to concrete crushing at the end of the beam in the 3rd cycle of drift ratio of 4.5%. In addition, the ductility (μ_e) of all the specimens was higher than that of the intermediate RC moment frame specified by the ASCE (2010).

• A comparative analysis of the structural performance of the specimens based on various indices (e.g., $StrI_i$, $StiI_i$ and $\beta_{ACI,i}$) revealed that the two specimens were very similar in regards to the column overstrength factor, energy dissipation performance, strength performance, and stiffness performance.

• The acceptance criteria of the ACI 374.1 report were partially met. The WB-H specimen failed to meet the stiffness degradation criterion (i.e., ACI 374.1 report 9.1.3-1) in the 3rd cycle of drift ratio of 3.5% in all load directions. This is because a bond degradation of the center reinforcing bar at the beam section occurred because of the shear lag effect; thus, the center reinforcing bar underwent a relatively higher strain relative to the outermost reinforcing bar at the high loading step (i.e., $\Delta \geq \Delta_y$). In contrast, the WB-S specimen in which all bottom reinforcing bars penetrated inside the column was found to partially meet the acceptance criteria of the ACI 374.1 report 9.1.3-1, as the slip of the reinforcing bars was relatively small compared to the WB-H specimen.

• The loading protocol reflecting the time history of ground motions is very important for more realistic seismic risk assessment of the proposed PC-WB joint. For further verification of seismic performances of target structures with the PC-WB joints, the shaking table test considering ground motions in the target seismic zone is suggested to be performed in the future.

Acknowledgments

This work was financially supported by Korea Ministry of Land, Infrastructure and Transport(MOLIT) as [Innovative Talent Education Program for Smart City]. Also, the first and second authors would like to acknowledge that this research was supported by the DL Construction Co., Ltd.

References

ACI Committee 318 (2019), *Building Code Requirements for Structural Concrete and Commentary (ACI 318-19)*, American Concrete Institute, Farmington Hills, MI.

ACI Committee 374 (2005), *Acceptance Criteria for Moment Frames Based on Structural Testing and Commentary (ACI 374.1-05)*, American Concrete Institute, Farmington Hills, MI.

ACI Committee 374 (2013), *Guide for Testing Reinforced Concrete Structural Elements under Slowly Applied Simulated Seismic Loads (ACI 374.2R-13)*, American Concrete Institute, Farmington Hills, MI.

Al-Osta, M.A., Khan, M.I., Bahraq, A.A. and Xu, S.Y. (2020), "Application of ultra-high performance fiber reinforced concrete for retrofitting the damaged exterior reinforced concrete beam-column joints", *Earthq. Struct.*, **19**(5), 361-377. https://dx.doi.org/10.12989/eas.2020.19.5.361.

Catalan, A., Benavent-Climent, A. and Cahis, X. (2010), "Selection and scaling of earthquake records in assessment of structures in low-to-moderate seismicity zones", *Soil Dyn. Earthq. Eng.*, **30**, 40-49.

https://doi.org/10.1016/j.soildyn.2009.09.003.

Arockiasamy, M., Badve, A.P., Rao, B.V. and Reddy, D.V. (1991), "Fatigue strength of joints in a precast prestressed concrete double tee bridge", *PCI J.*, **36**, 84-99. https://doi.org/10.15554/pcij.01011991.84.97.

ASCE (2010), *Minimum Design Loads for Buildings and Other Structures (ASCE/SEI 7-10)*, American Society of Civil Engineers, Reston, VA.

Behnam, H., Kuang, J.S. and Samali, B. (2018), "Parametric finite element analysis of RC wide beam-column connections", *Comput. Struct.*, **205**(1), 28-44. https://doi.org/10.1016/j.compstruc.2018.04.004.

Benavent-Climent, A. (2007), "Seismic behavior of RC wide beam-column connections under dynamic loading", *J. Earthq. Eng.*, **11**(4), 493-511. https://doi.org/10.1080/13632460601064814.

Chiu, C.K., Sung, H.F., Chi, K.N. and Hsiao, F.P. (2019), "Experimental quantification on the residual seismic capacity of damaged RC column members", *Int. J. Concrete Struct. Mater.*, **13**(3), 363-384. https://doi.org/10.1186/s40069-019-0361-0.

Choi, S.H., Hwang, J.H., Lee, D.H., Kim, K.S., Zhang, D. and Kim, J.R. (2018), "Experimental study on RC frame structures strengthened by externally-anchored PC wall panels", *Comput. Concrete*, **22**(4), 383-393. https://doi.org/10.4334/jkci.2015.27.4.451.

Dabiri, H., Kheyoroddin, A. and Kaviani, A. (2019), "A numerical study on the seismic response of RC wide column-beam joints", *Int. J. Civil Eng.*, **17**(7), 1-20. https://doi.org/ 10.1007/s40999-018-0364-2.

Elsouri, A.M. and Harajli, M.H. (2015), "Interior RC wide beam-narrow column joints: potential for improving seismic resistance", *Eng. Struct.*, **99**, 42-55. https://doi.org/ 10.1016/j.engstruct.2015.04.020.

Eurocode 8 (2004), *Design of Structures for Earthquake Resistance-Part 1: General, Seismic Actions, Rules for Buildings*, Committee Europpen de Normailsation, Brussels.

Fadwa, I., Ali, T.A., Nazih, E. and Sara, M. (2014), "Reinforced concrete wide and conventional beam-column connections subjected to lateral load", *Eng. Struct.*, **76**, 34-48. https://doi.org/ 10.1016/j.engstruct.2014.06.029.

Gentry, R. and Wight, J.K. (1994), "Wide beam-column connections under earthquake-type loading", *Earthq. Spectra*, **10**(4), 675-703. https://doi.org/ 10.1193/1.1585793.

Gunasekaran, U. and Ahmed, S.M. (2014), "Experimental investigation into the seismic performance of slabs in RC frame joints", *Mag. Concrete Res.*, **66**(15), 770-788. https://doi.org/ 10.1680/macr.13.00329.

IBC (2018), *International Building Code (IBC-2018), International Code Council*, Country Club Hills, U.S.A.

Karayannis, G.G. and Golias, E. (2018), "Full scale tests of RC joints with minor to moderate seismic damage repaired using C-FRP sheets", *Earthq. Struct.*, **15**(6), 617-627. https://doi.org/ 10.12989/eas.2018.15.6.617.

Kim, J.H., Choi, S.H., Hwang, J.H., Jeong, H., Han, S.J. and Kim, K.S. (2021), "Experimental study on lateral behavior of post-tensioned precast beam-column joints", *Struct.*, **33**(1), 841-854. https://doi.org/ 10.1016/j.istruc.2021.04.095.

Kuang, J.S., Behnam, H. and Huang, Q. (2016), "Effective beam width of reinforced-concrete wide beam-column connections", *Struct. Build.*, 1500124, 1-18. https://doi.org/10.1680/jstbu.15.00124.

Kulkarni, S.A. and Li, B. (2009), "Seismic behavior of reinforced concrete interior wide-beam column joints", *J. Earthq. Eng.*, **13**, 80-99. https://doi.org/10.1080/13632460802211941.

Li, B. and Kulkarni, A. (2010), "Seismic behavior of reinforced concrete exterior wide beam-column joints", *J. Struct. Eng.*, **136**(1), 26-36. https://doi.org/10.1061/(ASCE)0733-9455(2010)136:1(26).

Mejia-McMaster, J.C. and Park, R. (1994), "Test on special reinforcement for the end support of hollow-core slabs", *PCI J.*, **39**, 90-105. https://doi.org/10.15554/pcij.09011994.90.105.

Mirzabagheri, S., Tasnimi, A.A. and Mohammadi, M.S. (2016), "Behavior of interior RC wide and conventional beam-column roof joints under cyclic load", *Eng. Struct.*, **111**(15), 333-344. https://doi.org/10.1016/j.engstruct.2015.12.011.

Moon, J.H., Choi, Y.C., Lim, J.H., Lee, L.H., Kwon, K.H. and Kim, K.S. (2007), "Post-tensioned interior precast wide beam-column connections subjected to lateral loading", *Adv. Struct. Eng.*, **10**(5), 487-500. https://doi.org/10.1260/136943307782417654.

Natio, C.J., Cao, L. and Peter, W. (2009), "Precast concrete double-tee connections, part 1: tension behavior", *PCI J.*, **54**, 49-66. https://doi.org/10.15554/pcij.01012009.49.66.

Nguyen, X.H., Le, D.D., Nguyen, Q.H. and Nguyen, H.Q. (2020), "Seismic performance of RCS beam-column joints using fiber reinforced concrete", *Earthq. Struct.*, **18**(5), 599-607. https://dx.doi.org/10.12989/eas.2020.18.5.599.

NZS 3101 (2006), *New Zealand Standard Code of Practice for the Design of Concrete Structures*, Standards Association of New Zealand, Wellington.

Quintero-Febres, C.G. and Wight, J.K. (2001), "Experimental study of reinforced concrete interior wide beam-column connections subjected to lateral loading", *ACI Struct. J.*, **98**(4), 572-582. https://doi.org/10.14359/10300.

Rai, D.C. (2001), "Slow cyclic testing for evaluation of seismic performance of structural components", *ISET J. Earthq. Tech.*, **38**(1), 31-55.

Rosenthal, I. (1978), "Full scale test of continuous prestressed hollow-core slab", *PCI J.*, **23**, 74-81. https://doi.org/10.15554/pcij.05011978.74.81.

Siah, W.L., Stehle, J.S., Mendis, P. and Goldsworthy, H. (2003), "Interior wide beam connections subjected to lateral earthquake loading", *Eng. Struct.*, **25**(3), 281-291. https://doi.org/ 10.1016/S0141-0296(02)00150-5.

Tan, K.H., Zheng, L.X. and Paramasivam, P. (1996), "Designing hollow-core slabs for continuity", *PCI J.*, **41**, 82-91. https://doi.org/10.15554/pcij.01011996.82.91.

Turker, K. and Gungor, I. (2018), "Seismic performance of low and medium-rise RC buildings with wide-beam and ribbed-slab", *Earthq. Struct.*, **15**(4), 383-393. https://dx.doi.org/10.12989/eas.2018.15.4.383.

Yang, Y., Yang, C., Chen, Z., Wang, N. and Yu, Y. (2018), "Experimental study on seismic behavior of RC beam-column joints retrofitted using prestressed steel strips", *Earthq. Struct.*, **15**(5), 499-511. https://dx.doi.org/10.12989/eas.2018.15.5.499.

Zhang, H., Li, C., Wang, Z.F. and Zhang, C.Y. (2020), "Seismic performance assessments of precast energy dissipation shear wall structures under earthquake sequence excitations", *Earthq. Struct.*, **18**(2), 147-162. https://dx.doi.org/10.12989/eas.2020.18.2.147.

DK